Graphite-Supported Platinum Catalysts: Effects of Gas and Aqueous Phase Treatments

J. H. Vleeming,* B. F. M. Kuster,*,[1] G. B. Marin,* F. Oudet,† and P. Courtine‡

*Laboratorium voor Chemische Technologie, Schuit Institute of Catalysis, Eindhoven University of Technology, P.O. Box 513, 5600 MB Eindhoven, The Netherlands; †Service d' Analyse Physico-Chimique, Université de Technologie de Compiègne, Centre de Recherches de Royallieu, P.O. Box 649, 60206 Compiègne Cedex, France; and ‡Départment de Génie Chimique, Université de Technologie de Compiègne, Centre de Recherches de Royallieu, P.O. Box 649, 60206 Compiègne Cedex, France

The effects on the platinum particle diameter and the available platinum surface area of a graphite-supported platinum catalyst resulting from pretreatments and from performing a selective oxidation reaction are investigated. In the gas phase considerable catalyst sintering occurs only in the presence of oxygen at 773 K due to extensive carbon burn-off, whereas in an aqueous phase platinum particle growth is limited upon oxidative treatment. A hydrogen treatment in aqueous phase at 363 K causes platinum particle growth, aggregate formation, and covering of metal sites. These phenomena become more important with increasing pH. Platinum particle growth and aggregate formation are attributed to platinum particle rather than platinum adatom mobility and is caused by the destruction of the oxygen-containing surface groups on the graphite support, which serve as anchorage sites for the platinum particles. Site covering is caused by products originating from the graphite support, which are formed as a result of the reductive treatments. When performing the aqueous phase oxidation of methyl α-D-glucopyranoside at 323 K and a pH of 9, catalyst modifications are small under oxidative conditions. Exposure of the catalyst for several hours to methyl α-D-glucopyranoside under the same conditions but in the absence of oxygen causes site covering. © 1997 Academic Press

INTRODUCTION

Partial oxidations of alcohols or carbohydrates are interesting processes for the production of valuable chemicals. The oxidation of primary alcohols to aldehydes or carboxylic acids and of secondary alcohols to ketones can be performed with molecular oxygen in aqueous media over supported platinum and palladium catalysts (1–4). Especially for carbohydrate chemistry the mild reaction conditions and high selectivity are very attractive. However, catalyst deactivation is often reported and forms the major bottleneck for the commercialization of these processes. Four deactivation mechanisms can be distinguished:

(i) Deactivation by over-oxidation or oxygen poisoning has received the most attention. It has been reported for the oxidation of primary alcohols (5–10), secondary alcohols (8, 10–12), and carbohydrates (10, 13–19). It is generally accepted that over-oxidation is caused by the strong adsorption of oxygen or oxygen-containing species at the platinum surface (16–18, 20, 21). The catalyst activity is easily recovered by a mild in-situ reduction (11, 13–16, 18) or is avoided by regulation of the oxygen supply (3, 4), application of diffusion-stabilized catalysts (3, 4), or the addition of promoter metals to the platinum catalyst (9, 10).

(ii) Covering of adsorption sites ("site covering") by major products or minor side products is frequently reported as a cause of deactivation. In the field of carbohydrate oxidation product adsorption was found to deactivate the catalyst for the oxidation of D-glucose (22) and D-gluconic acid (23) in acidic media. In electrochemical oxidations of alcohols in acidic media, CO from aldehyde intermediates was found to cover active sites (7, 24, 25), but no CO poisoning was observed for D-glucose oxidation (22). In alkaline media CO is oxidized under reaction conditions (4) and is present in small amounts (26). In neutral or alkaline media side products may be produced, often via aldol dimerization or polymerization, which may cover irreversibly the active site (4–6, 11, 12). Also, during the initial reductive pretreatment of the catalyst in aqueous media, which is often performed in the presence of the alcohol or carbohydrate to be oxidized, the platinum surface is covered by dehydrogenation products (4, 10, 18, 19). Subsequent oxidation removes poisoning species such as CO (4), but other side products may still cover active sites (19).

(iii) Metal leaching, the loss of an active metal via the dissolution of metal ions, often constitutes the main reason why a process is not commercially feasible. Especially in the presence of certain anions or complexing agents like carbohydrates and their oxidation products, dissolution of metals is enhanced (4, 16, 19). Dissolution and loss of active metal is not frequently reported, because many oxidations are carried out in batch reactors for relatively short reaction

[1] To whom correspondence should be addressed. E-mail: margriet@chem.tue.nl.

148

times. However, upon re-use of the catalyst (8) or after careful characterization of used catalysts or analysis of the liquid phase (10, 18, 19), a decrease of the catalyst metal content was observed. During continuous oxidation of methyl α-D-glucopyranoside to sodium methyl α-D-glucuronate a platinum content of 2–4 ppm was measured in the solution (16).

(iv) Metal particle growth, just like metal leaching, is observed only after prolonged oxidation. Schuurman *et al.* (16) explain the irreversible deactivation observed for the oxidation of methyl α-D-glucopyranoside as being the result of recrystallization via dissolution and subsequent redeposition of platinum ions. In this so-called Ostwald ripening mechanism large particles grow at the expense of smaller ones, resulting in an increase of the average metal particle diameter (27). Other mechanisms have been proposed such as two-dimensional Ostwald ripening, a mechanism in which platinum atoms migrate on the support surface (28), or an electro-recrystallization mechanism in which local cells are formed between large and small platinum particles, causing platinum ion complex migration compensated by electron transport over the support surface (29).

The aim of this paper is to describe the effects of different environments and reaction conditions on a platinum-on-graphite catalyst in terms of site covering and particle growth. Particle growth is studied by transmission electron microscopy (TEM) and X-ray diffraction (XRD). Site covering can be derived from CO chemisorption, when the results are compared to TEM and XRD. Deactivation is often only clearly observed after prolonged use of the catalyst. Therefore gas phase and aqueous phase treatments of the platinum-on-graphite catalyst are performed under extreme conditions to accelerate site covering and particle growth. The mechanisms for site covering and particle growth observed as a result of these treatments are compared to the deactivation observed for the continuous oxidation of methyl α-D-glucopyranoside to sodium 1-O-methyl glucuronate.

EXPERIMENTAL

Fresh Catalyst

The fresh platinum on a high-surface-area graphite catalyst (Pt/HSAG) was prepared according to the procedure of Richard and Gallezot (30). Batches of 8×10^{-3} kg HSAG (Johnson Matthey, CH10213) with a BET surface area of 2.89×10^5 m^2 kg^{-1} were activated in air at a flow rate of 5×10^{-6} Nm^3 s^{-1} at 773 K for 5 h, resulting in a carbon burn-off of 21 wt%. The air-oxidized graphite was stirred in a 13 wt% sodium hypochlorite solution (Janssen p.a.) at a concentration of 80 kg m^{-3} for 24 h at room temperature. The graphite was carefully washed with ultra pure Millipore water (18 MΩ cm), which was used for all preparations, aqueous phase treatments, and reactions. The graphite was

filtered on a 0.45-μm Millipore filter and dried at 323 K and 5 kPa. Competitive ion-exchange was used by drop-wise adding a 16 wt% tetrammine platinum hydroxide solution, Pt(NH$_3$)$_4$(OH)$_2$ (Degussa), to 50 kg m^{-3} graphite in 1 M ammonia (Merck p.a.) until a platinum concentration of 10 kg m^{-3} was reached. The alkaline solution was stirred for 24 h at room temperature. The catalyst was carefully washed, filtered on a 0.45-μm filter, dried at 323 K and 5 kPa, and reduced in batches of 8×10^{-3} kg in hydrogen at a flow rate of 5×10^{-6} Nm^3 s^{-1} at 573 K for 3 h. The platinum content amounted to 3.4 wt% and the BET surface area was 1.02×10^5 m^2 kg$_{\text{cat}}^{-1}$.

Gas Phase Treatments

The fresh catalyst was treated by heating 2.5×10^{-4} kg in hydrogen, nitrogen, or air at a flow rate of 5×10^{-6} Nm^3 s^{-1} at 773 K for 2 h. Treatment in air was followed by reduction in hydrogen at 573 K for 1 h. After treatment in hydrogen and nitrogen the increase of the platinum content was negligible, whereas, after treatment in air the platinum content had increased by a factor of four, due to platinum-catalyzed carbon burn-off (31).

Aqueous Phase Treatments

A 4×10^{-4} m^3 stirred glass tank reactor equipped with a glass stirrer was filled with 2.5 to 10 kg m^{-3} fresh catalyst in 0.2×10^{-3} m^3 Millipore water (pH $\approx$ 7), 100 mol m^{-3} HClO$_4$ (pH = 1), or 100 mol m^{-3} NaOH (pH = 13). The slurry was stirred in a nitrogen or hydrogen atmosphere at 363 K or in an oxygen atmosphere at 323 K at a gas flow rate of 3×10^{-6} Nm^3 s^{-1}.

Oxidation of Methyl α-D-Glucopyranoside: Equipment and Procedure

A continuous flow three-phase slurry reactor of 0.7×10^{-3} m^3 volume was used. The glass reactor was equipped with a glass stirrer with internal gas circulation, a pH electrode (Radiometer PHC2402), an oxygen electrode (Ingold 341003005), and a membrane filter of 0.45 μm (Millipore GVWP09050) to retain the catalyst. The temperature was measured with a Pt-100 probe and controlled by a water bath (Beun de Ronde CS6 and R22). The reactor was operated at atmospheric pressure at a constant gas flow rate of 3×10^{-6} Nm^3 s^{-1}.

Before the start of the oxidation reaction 0.7×10^{-3} kg fresh catalyst was prereduced in 0.35×10^{-3} m^3 water at 363 K for 1.8×10^3 s in a hydrogen flow. Under a nitrogen atmosphere the reactor was cooled to 323 K and the water was removed. A solution of methyl α-D-glucopyranoside (Fluka) and sodium methyl α-D-glucuronate was added, which was previously prepared by a separate batch oxidation reaction of methyl α-D-glucopyranoside under identical reaction conditions and stopped at the same conversion level as the reaction to be performed. The reaction was

started by replacing the nitrogen flow with an oxygen flow. The methyl α-D-glucopyranoside and sodium hydroxide solutions were added to the reactor simultaneously at equal flow rates with a tubing pump (Masterflex 7523-35) equipped with two equal pump heads. The inlet liquid flow rate was adapted to the rate of production of sodium 1-o-methyl glucuronate by a feedback PID-control (Eurotherm 940D) based on the pH measurement of the reaction mixture. In this way the concentration of methyl α-D-glucopyranoside and sodium methyl α-D-glucuronate were kept constant despite catalyst deactivation, provided that catalyst deactivation did not result in selectivity changes. Analysis of the reaction mixture, performed off-line with a HPLC analysis described elsewhere (16), confirmed that the concentrations of methyl α-D-glucopyranoside and sodium methyl α-D-glucuronate were constant throughout the reaction. The carbon balance was kept within 1% at the applied conversion level. The inlet liquid flow rate was measured by recording the weight loss of the liquid supply vessels with two Sartorius I8100P balances. The outlet liquid flow rate was controlled via PID-control (Eurotherm 940D) of a tubing pump (Masterflex). This controller takes as input the differential pressure (Fischer & Porter 50DPF100-3) between the head space and the bottom (tip of the immersion pipe) of the reactor. In this way the total liquid volume of the reactor was kept constant within 5×10^{-6} m^3. The stirrer speed during reaction was 25 s^{-1}, ensuring good contact of the three phases. It was verified that the kinetic measurements were free of mass and heat transfer limitations.

Regeneration of the catalyst to overcome over-oxidation was performed *in situ*. The oxygen flow was successively replaced by nitrogen, hydrogen, and nitrogen for 1.8×10^3 s. The pH, temperature, and concentrations were maintained constant during regeneration.

Catalyst Characterization

Catalyst samples from liquid phase experiments were filtered on a 0.45 μm membrane filter (Schleicher and Schull RC55 or Millipore GVWP09050), carefully washed with Millipore water and dried at 323 K and 5 kPa.

The platinum content of the catalysts was determined in duplicate by dissolving the platinum in concentrated HCl/HNO$_3$ (3:1, Merck p.a.) followed by the removal of the nitric acid by adding hydrochloric acid and evaporating three times. A yellow platinum tin chloride complex was formed by adding a hydrochloric acid containing tin chloride solution (Merck p.a.) and the extinction was measured at 403 nm (32, 33). The standard deviation was found to be smaller than 0.1 wt% for all measurements. The platinum concentration in the liquid phase was determined from the extinction of the platinum tin chloride complex, which was measured at 403 nm with a diode-array detector with a detection limit of 1×10^{-4} mol m^{-3}.

The specific surface area was measured as the BET surface area with a Micromeritics ASAP2000 instrument. An exact amount of catalyst or graphite support was dried at 383 K for 1 h under vacuum in the sample tube prior to measurement.

The fraction of platinum atoms exposed was determined by CO pulse chemisorption using a modified gas chromatograph (Carlo Erba 4300) equipped with a thermal conductivity detector (TCD). Hydrogen and helium were purified by an oxygen and moisture filter and the carbon monoxide (99.997%) was used without further purification. Prior to measurement all catalyst samples were dried at 323 K at 5 kPa overnight. An exact amount of catalyst was reduced in a Pyrex glass plug flow reactor at 373 K for 2×10^3 s in 3×10^{-7} Nm^3 s^{-1} hydrogen. CO was adsorbed in a helium flow of 3×10^{-7} Nm^3 s^{-1} at 273 K. The fraction exposed, FE^{CO}, was calculated assuming an adsorption stoichiometry of CO$_{ads}$:Pt$_s$ = 1. Every catalyst sample was measured in duplicate according to the procedure described above. The standard deviation for the obtained FE^{CO} was smaller than 0.01 for all measurements.

Transmission electron microscopy (TEM) micrographs were obtained with a JEOL 1200 EX microscope. The samples were ultrasonically dispersed in tetrachloromethane p.a. or ethanol p.a. and the suspension was brought onto 400 mesh copper grids coated with a carbon support film (TAAB). An accelerating potential of 120 kV was used with a microscope magnification between 50,000 and 500,000. The resulting micrographs were analyzed with a scale magnifying glass (Peak) with a magnification of 10 and an accuracy of 0.1 mm to obtain the platinum particle diameter distribution. Depending on the quality of the micrographs and the magnification applied, between 169 and 569 platinum particles were counted per catalyst sample.

The underlined number, surface area, and weight averaged platinum particle diameter were determined from the distribution according to Lemaître *et al.* (34).

$$d_n^{TEM} = \frac{\sum_i n_i d_i}{\sum_i n_i}; \qquad d_s^{TEM} = \frac{\sum_i n_i d_i^3}{\sum_i n_i d_i^2};$$

$$d_w^{TEM} = \frac{\sum_i n_i d_i^4}{\sum_i n_i d_i^3} \qquad [1]$$

The sample standard deviation for the number, surface area, and weight averaged platinum particle diameter is obtained from:

$$\sigma_n = \sqrt{\frac{\sum_i n_i (d_i - d_n)^2}{\sum_i n_i}}; \qquad \sigma_s = \sqrt{\frac{\sum_i n_i d_i^2 (d_i - d_s)^2}{\sum_i n_i d_i^2}};$$

$$\sigma_w = \sqrt{\frac{\sum_i n_i d_i^3 (d_i - d_w)^2}{\sum_i n_i d_i^3}} \qquad [2]$$

and the 95% confidence interval for d_j^{TEM} ($j =$ n, s, or w) is

$$d_j^{TEM} \pm \frac{1.96\,\sigma_j}{\sqrt{n}} \qquad [3]$$

X-ray diffraction (XRD) was performed unless the amount of catalyst was insufficient to fill the sample holder. XRD was determined using Cu K_α radiation ($\lambda =$ 0.15418 nm) and a CGR focusing monochromator (curved quartz single crystal). The curve position sensitive detector (INEL CPS120) had an angular range of 5–120° (2θ) and a resolution of approximately 0.03° (2θ). Spectra were recorded for 2.4×10^3 s in the reflection or transmission mode. For the line analysis and deconvolution SIEMENS/SOCABIM (FIT) software was used, as graphite lines partially overlapped the Pt(111) line. The average platinum particle diameter was calculated from the Warren-modified Scherrer equation (35):

$$d_w^{XRD} = \frac{0.9\,\lambda}{\Delta(2\theta)\cos\theta} \qquad \text{with } \Delta(2\theta) = \sqrt{\beta_{1/2}^2 - b^2} \quad [4]$$

with $\lambda = 0.15418$ nm, θ is the Bragg angle, $\beta_{1/2}$ is the linewidth at half maximum in radians, and $b = 0.00182$ radians (0.104°), the instrumental line broadening being determined experimentally with bulk platinum with high grain size.

Particles as small as 1.5 nm could be detected by line broadening analysis. In the review by Gallezot (35) other examples are mentioned, where particle diameters are established by line broadening analysis which are smaller than the generally accepted detection limit of about 4 nm. Sashital *et al.* (36) reported examinations with X-ray diffraction of platinum particles on silica as small as 2.5 nm and Bergeret *et al.* (37) established particle diameters as small as 1.5 nm by line broadening analysis. The accuracy of the measurement of such small particles is, of course, rather limited.

In order to compare the results obtained with XRD, TEM, and CO chemisorption, the exposed fraction determined by CO chemisorption, FE^{CO}, was converted to the surface-area-averaged particle diameter, d_s^{CO}, assuming hemispherical particles and 1.42×10^{19} platinum atoms per square meter (38):

$$d_s^{CO} = \frac{1.3 \times 10^{-9}}{FE^{CO}}. \qquad [5]$$

Obviously the application of Eq. [5] is only allowed when the platinum surface atoms are available for CO chemisorption, i.e., are not covered by adspecies on which CO does not chemisorb.

RESULTS

Fresh Catalyst

A TEM micrograph and the platinum particle diameter distribution of the fresh catalyst are presented in Figs. 1 and 2a, respectively. It is a well defined monodisperse catalyst in agreement with the results of Richard and Gallezot (30). The platinum particle diameter ranges from the detection limit to 2.5 nm. The results of the characterization of the fresh catalyst with TEM, CO chemisorption, and XRD are given in Table 1. With XRD a weight-averaged diameter, d_w, and with chemisorption techniques a surface-area-averaged diameter, d_s, are obtained from the exposed fraction of metal atoms (38). From the platinum particle diameter distribution obtained with TEM the number-averaged, surface-area-averaged, and weight-averaged diameters were calculated.

For the fresh catalyst the observed order is $d_n^{TEM} < d_w^{XRD} < d_s^{TEM} < d_w^{TEM} < d_s^{CO}$. This is in good agreement with the generally observed order $d_n^{TEM} < d_w^{XRD} < d_s^{chem}$. For example, Scardi and Antonucci (39) reported this order for platinum on carbon catalysts using cyclic voltammetry as the chemisorption technique, obtaining the platinum surface area from the Coulombic charge transferred during hydrogen adsorption.
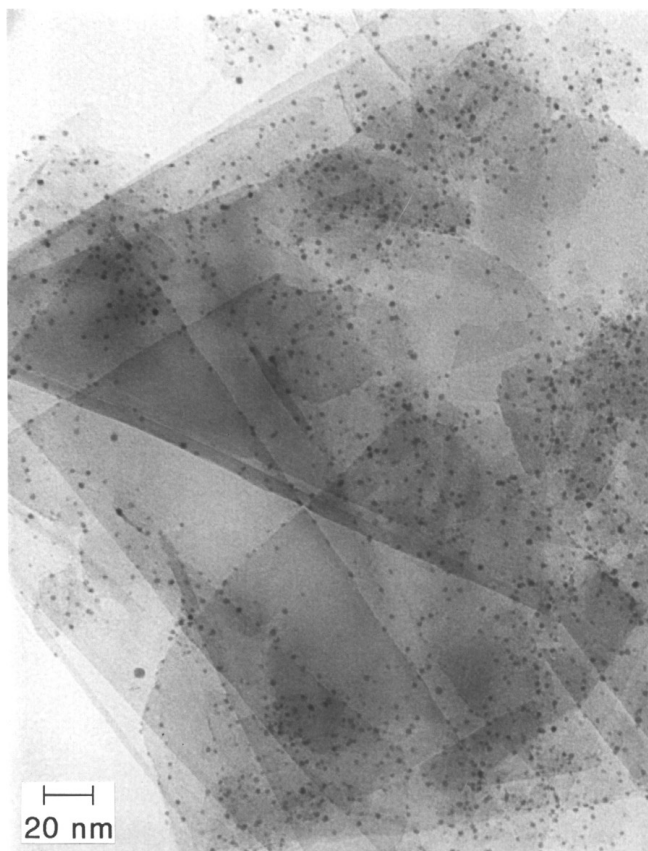

FIG. 1. Micrograph (TEM) of the fresh platinum on graphite catalyst.

The smaller diameter obtained with XRD compared to d_w^{TEM} may be attributed to the inaccuracy of line broadening analysis for small particles. The width of the XRD lines is affected by internal disorder and strain of the platinum particles (40), which is certainly found at the edges of the particles. For small particles this will mean a large decrease of the size of the reflecting crystalline structure. Furthermore, particles envisaged with TEM as one particle may actually consist of smaller crystalline structures. As a consequence d_w^{XRD} will be smaller than d_w^{TEM}.

The diameter obtained with CO chemisorption, d_s^{CO}, is larger than d_s^{TEM} for several possible reasons. First, the assumption of hemispherical particles and the amount of platinum atoms per surface area (1.42×10^{19} m^{-2} (38)) may be incorrect. Often a different constant is used in Eq. (5): $d = 1.08 \times 10^{-9}$/FE (41). Further, the assumed adsorption
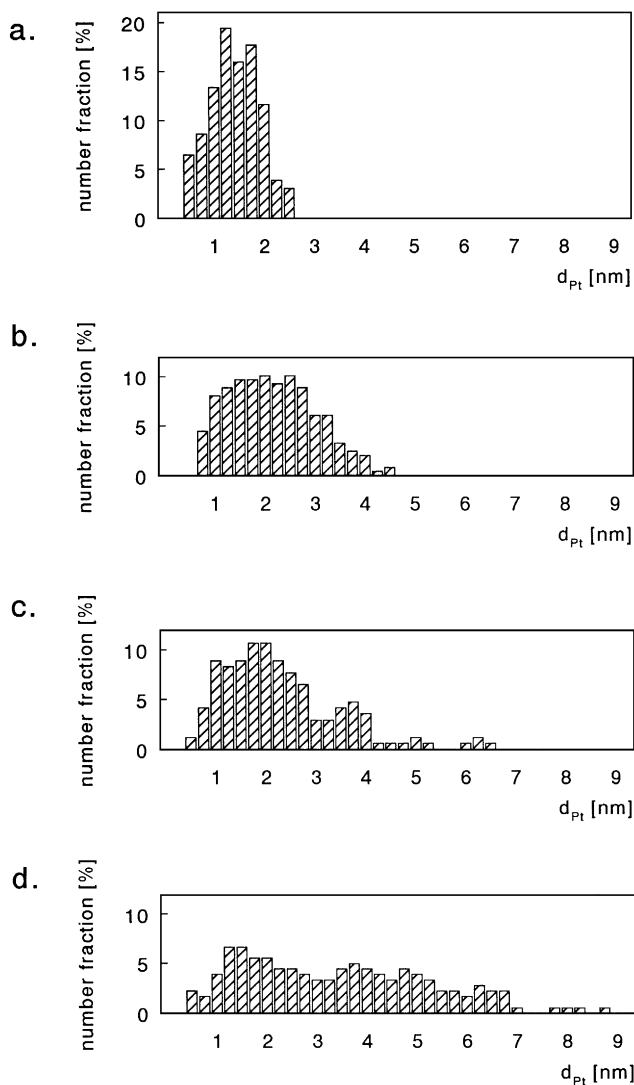
TABLE 1

The Number, Surface Area, and Weight-Averaged Platinum Particle Diameter Obtained by TEM (d_n^{TEM}, d_s^{TEM}, and d_w^{TEM}), the Fraction Exposed, and Platinum Particle Diameter Measured by CO Chemisorption (FE^{CO} and d_s^{CO}), and the Platinum Particle Diameter Measured by X-Ray Diffraction (d_w^{XRD})

Catalyst[a]	d_n^{TEM} [nm]	d_s^{TEM} [nm]	d_w^{TEM} [nm]	FE^{CO} $\left[\frac{mol_{Pt_s}}{mol_{Pt}}\right]$	d_s^{CO} [nm]	d_w^{XRD} [nm]
Fresh	1.45 ± 0.04	1.70 ± 0.04	1.81 ± 0.04	0.56	2.3	1.5[b]
H$_2$G	2.0 ± 0.1	2.9 ± 0.1	3.3 ± 0.1	0.60	2.2	—
N$_2$G	1.7 ± 0.1	2.4 ± 0.1	2.9 ± 0.1	0.57	2.3	—
O$_2$G	6.5 ± 0.4	14.0 ± 0.5	16.9 ± 0.5	0.09	14	25
H$_2$B1–0.3	2.2 ± 0.1	2.8 ± 0.1	3.0 ± 0.1	0.37	3.5	—
H$_2$B1–3.6	2.3 ± 0.2	3.5 ± 0.2	4.2 ± 0.2	0.26	5.0	—
H$_2$B1–250	3.4 ± 0.3	5.2 ± 0.3	5.7 ± 0.2	0.09	14	3.4
H$_2$B2–250	2.4 ± 0.2	3.9 ± 0.2	4.9 ± 0.3	0.18	7.2	3.1
H$_2$B2–250R	2.2 ± 0.2	3.7 ± 0.2	4.6 ± 0.2	0.25	5.2	—
H$_2$L	1.60 ± 0.05	1.90 ± 0.05	2.03 ± 0.04	0.41	3.2	1.6[b]
M1	1.39 ± 0.06	1.79 ± 0.06	1.95 ± 0.06	0.38	4.8	1.5[b]
M4	1.53 ± 0.05	1.88 ± 0.04	2.00 ± 0.04	0.42	3.1	1.7[b]
M7	1.64 ± 0.04	1.90 ± 0.04	2.02 ± 0.04	0.27	4.8	—

[a] The catalyst codes are explained in the text.
[b] Due to the determination by line broadening analysis the accuracy is limited.

stoichiometry of $CO_{ads}/Pt_s = 1$ is too large for small particles (41, 42).

Gas Phase Treatments

The growth of platinum particles upon heat treatment in the presence of a gas phase was investigated by heating the fresh catalyst at 773 K. Table 1 shows the results of this treatment in a hydrogen, nitrogen, and oxygen atmosphere, the catalyst samples being indicated by H$_2$G, N$_2$G, and O$_2$G. Heating in a hydrogen or nitrogen atmosphere results in a small increase of the average platinum particle diameter and a small decrease of the fraction exposed, FE^{CO}. Oxidation of the fresh catalyst in air results in a large increase of the average platinum particle diameter. This is caused by the platinum-catalyzed oxidation of the graphite support (31), resulting in a 75 wt% carbon burnoff. Because of this very high burnoff the support is destroyed, together with the anchorage sites of the platinum particles, and platinum particles will migrate over the support surface, collide, and coalesce. The effect of oxidation at 773 K on the diameter of the platinum particles is shown in Fig. 3, in which platinum particles with a diameter of up to 30 nm can be observed.

Aqueous Phase Treatments

Figure 4 shows the exposed fraction of platinum atoms after aqueous phase treatment of the fresh catalyst at pH = 1, 7, and 13 in a hydrogen and nitrogen atmosphere at 363 K and in an oxygen atmosphere at 323 K for 20 h. The FE^{CO}

FIG. 2. Platinum particle diameter distribution of the fresh catalyst (a) and after reductive treatment in a hydrogen atmosphere in 0.1 M NaOH (pH = 13) at 363 K for (b) 0.3×10^3, (c) 3.6×10^3, and (d) 2.5×10^5 s.
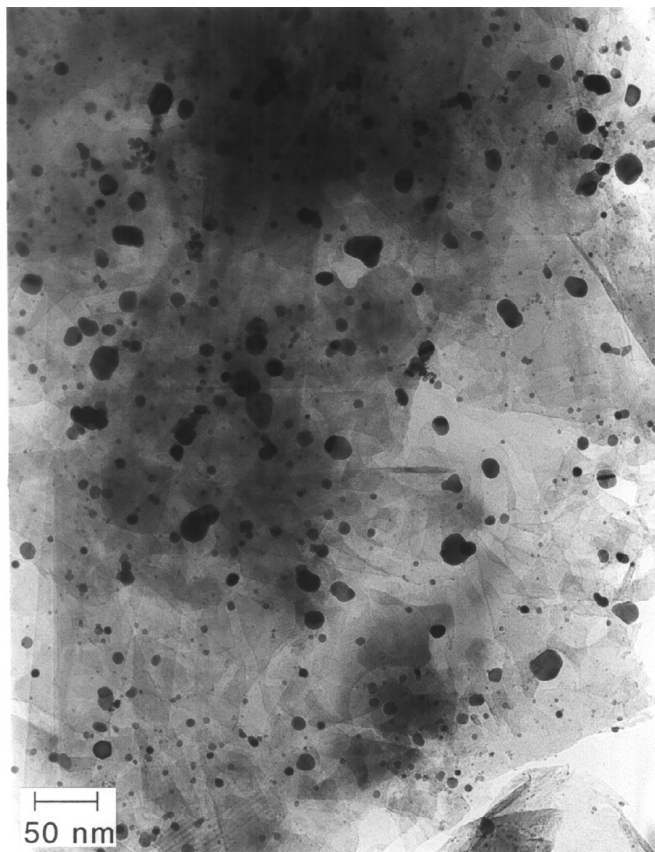
FIG. 3. Micrograph (TEM) of catalyst sample O_2G after oxidation in air at 773 K for 2 h.

decreases with increasing pH, the strongest effect being observed for hydrogen.

In order to study the effect of the hydrogen treatment at pH = 13 the fresh catalyst was treated for 250×10^3 s at a catalyst concentration of 5 kg m^{-3}. Figure 5 shows a sharp decrease of the exposed fraction of platinum atoms, FE^{CO}, as a function of time for this experiment. Three samples taken at 0.3, 3.6, and 250×10^3 s, indicated by H_2B1-0.3, H_2B1-3.6, and H_2B1-250, were also characterized with TEM and XRD. The results are listed in Table 1. The decrease of the FE^{CO} from 0.56 for the fresh catalyst to 0.09 after 250×10^3 s is accompanied by an increase of the average platinum particle diameter. With TEM a gradual increase from $d_s^{TEM} = 1.70$ to 5.2 nm is observed. The platinum particle diameter distributions of this experiment are depicted in Fig. 2 and it clearly demonstrates platinum particle growth. With XRD an increase from 1.5 to 3.4 nm was determined.

Another effect of the treatment at pH = 13 in a hydrogen atmosphere is the appearance of platinum aggregates. Figure 6 shows a TEM micrograph of the largest aggregate observed for H_2B1-250. The amount and size of these aggregates increases with increasing reduction time. It is not clear whether the aggregates consist of platinum exclusively or whether carbonaceous material is incorporated in
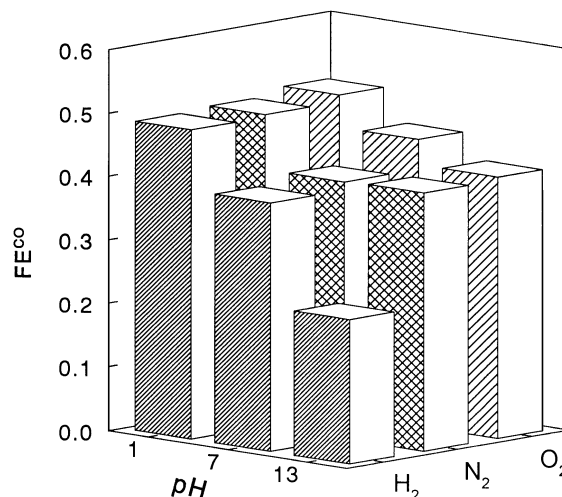

FIG. 4. Fraction exposed measured with CO chemisorption, FE^{CO}, as a function of the pH and atmosphere after a 20-h treatment at 363 K (H_2 and N_2) or 323 K (O_2).

the aggregates. EDX is not a helpful tool in this case because both the catalyst support and the film on the copper grid are composed of carbon, which contributes to the total carbon signal in the EDX spectrum.

Repeating the reduction experiment at a higher catalyst concentration of 10 kg m^{-3}, indicated by H_2B2-250 in Table 1, after 250×10^3 s the fraction exposed was 0.18. A series of treatments with H_2 at pH = 13 indicated that a higher NaOH/catalyst ratio resulted in a larger decrease of the fraction exposed. A NaOH consumption of 1 mol kg$_{cat}^{-1}$ or 6 mol mol$_{Pt}^{-1}$ was found for a catalyst concentration of 10 kg m^{-3}. The higher NaOH/catalyst ratio for H_2B1-250 compared to H_2B2-250 has led to a larger increase of the platinum particle diameter as measured with TEM and XRD and a smaller FE^{CO}, as is clear from Table 1. Also,
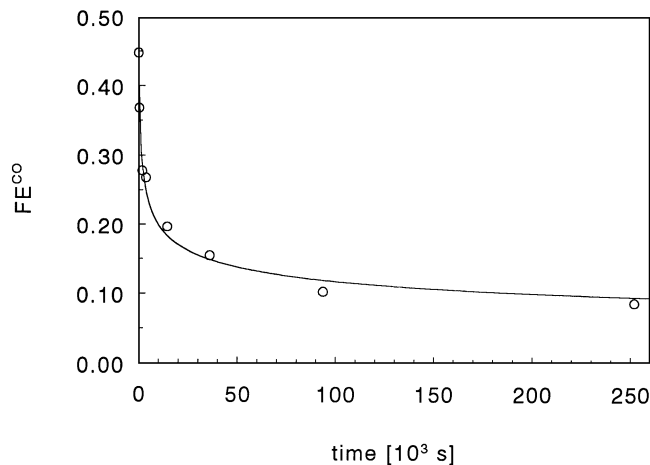

FIG. 5. Fraction exposed measured with CO chemisorption, FE^{CO}, upon reductive treatment in a hydrogen atmosphere in 0.1 M NaOH (pH = 13) at 363 K as a function of time.
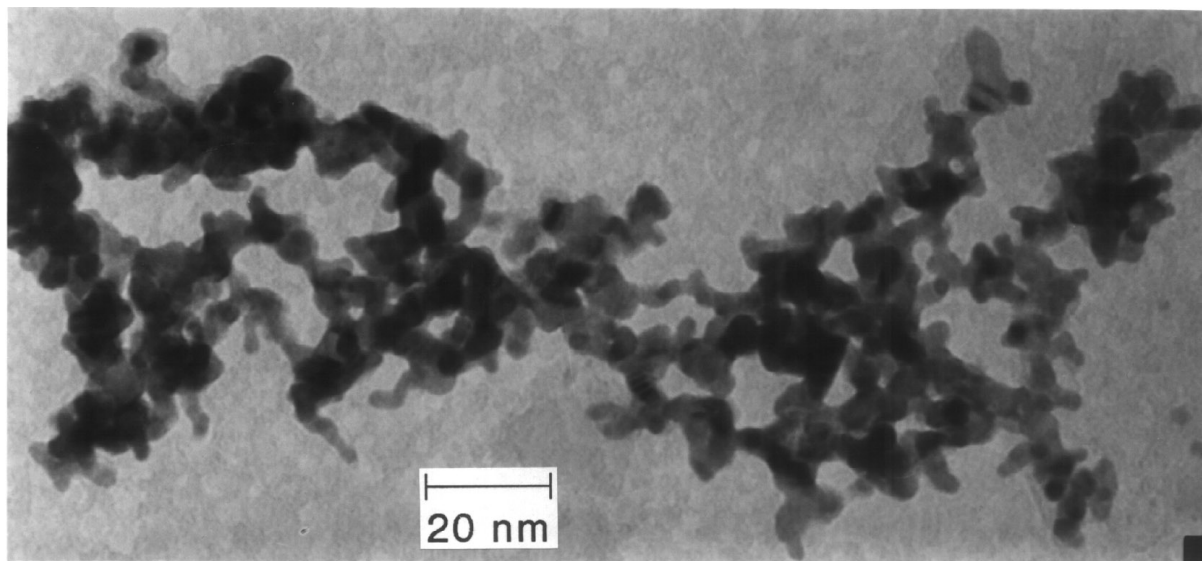
FIG. 6. Micrograph (TEM) of the largest platinum aggregate observed after reductive treatment of the fresh catalyst in a hydrogen atmosphere in 0.1 M NaOH (pH = 13) at 363 K for 2.5×10^5 s.

larger platinum aggregates were observed on the former sample with TEM.

Next, H$_2$B2-250 was treated in 100 mol m^{-3} HClO$_4$ at 323 K by applying 4 oxidation reduction cycles indicated in Table 1 as H$_2$B2-250R. The FE^{CO} recovered to 0.25. Another indication that site coverage and particle growth occur simultaneously during treatment with H$_2$ at pH = 13 is the fact that the increase of the d_s^{CO} from 2.3 nm for the fresh catalyst to 14 nm for H$_2$B1-250 is much larger than the increase of the d_s^{TEM} from 1.70 to 5.2 nm and the d_w^{XRD} from 1.5 to 3.4 nm. Note that it was difficult to measure the average platinum particle diameter with TEM, because of the irregular shape of the platinum particles and the presence of clusters of particles forming aggregates. This may explain why d_w^{TEM} is larger than d_w^{XRD} for H$_2$B1-250 and H$_2$B2-250.

It was verified whether the catalyst was poisoned by impurities originating from the reactor, because after several treatments under hydrogen at pH = 13 at 363 K corrosion of the glass was observed. Combination of energy dispersive x-ray analysis, EDX, with TEM or scanning transmission electron microscopy, STEM, could not reveal the presence of impurities, e.g. silicon, when characterizing platinum particles or aggregates of H$_2$B1-250.

Oxidation of Methyl α-D-Glucopyranoside

The oxidation reaction of methyl α-D-glucopyranoside to 1-o-methyl α-D-glucuronate is shown in Fig. 7. Figure 8 shows the initial specific consumption rate, R_w^0, as a function of the number of oxidation runs and the number of overnight N$_2$ treatments. During each run the rate decreased due to overoxidation (16, 18). Regeneration of the catalyst after 10×10^3 s reaction by replacing the oxygen flow by nitrogen and hydrogen for 1.8×10^3 s and resum-

ing the oxygen feed results in the complete recovery of the initial rate in the next oxidation run. Complete recovery was not observed if the catalyst was kept under nitrogen overnight in the reaction solution at 323 K for 50×10^3 s prior to the regeneration. This is clear in Fig. 8 from the decrease of the initial rate with an increase of the number of overnight N$_2$ treatments.

Extension of the oxidation time to 40×10^3 s during oxidation run 2 after two overnight N$_2$ treatments did not result in a change of the initial rate after regeneration. Consequently it is concluded that deactivation during oxidation caused by platinum particle growth and site coverage can be neglected and that the deactivation as a result of two overnight N$_2$ treatments is not recovered.

Deactivation due to platinum leaching could be neglected. The platinum ion concentration in the reactor solution was measured 11 times during the experiment both at the beginning and the end of an oxidation run. No effect of the run time on the platinum ion concentration was observed. The average platinum ion concentration amounted to $0.6 \pm 0.1 \times 10^{-3}$ mol m^{-3} (0.12 ppm). This concentration corresponds to a total loss of 1% of the amount of platinum present. During the oxidation of methyl α-D-glucopyranoside Schuurman *et al.* (16) measured a higher platinum concentration of 10–20×10^{-3} mol m^{-3} (2–4 ppm).
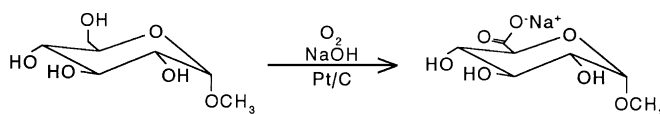

FIG. 7. The oxidation reaction of methyl α-D-glucopyranoside to sodium 1-o-methyl glucuronate with molecular oxygen over a platinum catalyst.

The results of the characterization of three samples which were used for the oxidation of methyl α-D-glucopyranoside are listed in Table 1 and denoted by M1, M4, and M7. The number indicates the number of intermediate regenerations with N_2 and H_2 for 1.8×10^3 s. Prior to each experiment the catalyst was reduced at 363 K in water. The catalyst characterization results after this prereduction are listed in Table 1 as H_2L.

From Table 1 it can be concluded that the increase of the platinum particle diameter of the catalysts used for the methyl α-D-glucopyranoside oxidation is small compared to the fresh catalyst and that no further increase is observed after the prereduction. The fraction exposed, which decreased after prereduction from 0.56 to 0.41, remained constant for M1 and M4 which were not treated overnight, whereas for M7 it decreased further to 0.27. At equal platinum particle diameter this decrease must be attributed to site covering, which is caused by the overnight storage in nitrogen atmosphere and corresponds to the decrease of the initial rates in Fig. 8 after each overnight N_2 treatment.

From the TEM micrographs of catalysts used for reaction or the pre-reduced sample H_2L another form of irreversible deactivation was observed, which was already mentioned for the experiments in which the catalyst was treated in a hydrogen atmosphere at high temperature and high pH. In Fig. 9 the TEM micrograph of catalyst sample M7 is given. Small platinum aggregates like the ones observed for the aqueous phase hydrogen-treated catalyst H_2B1-250 appear.
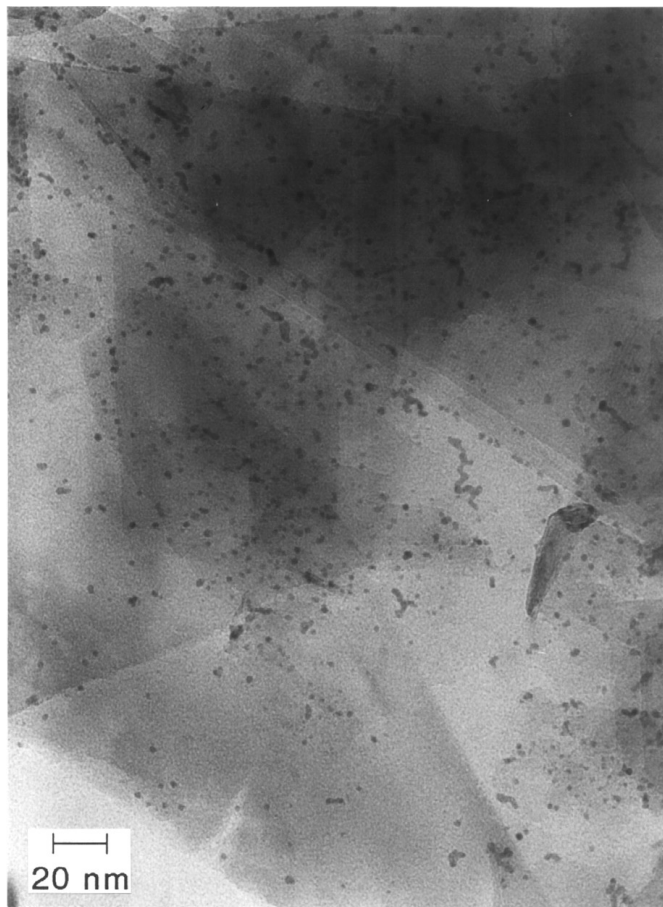

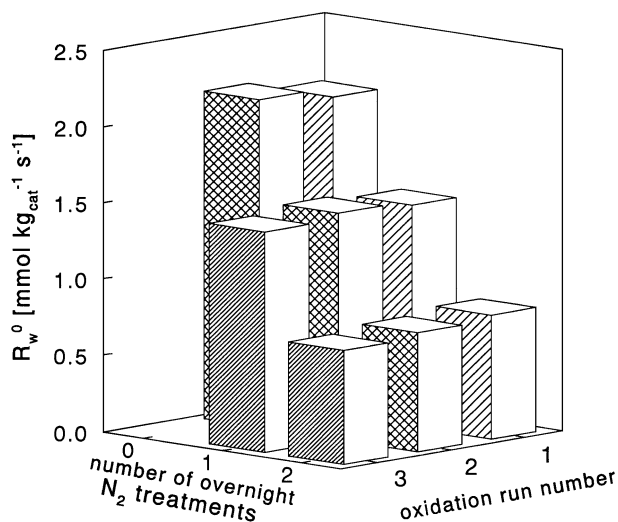FIG. 9. Micrograph (TEM) of catalyst sample M7 after the oxidation reaction of methyl α-D-glucopyranoside.

FIG. 8. The initial rate of consumption of sodium hydroxide, R_w^0, for the oxidation of methyl α-D-glucopyranoside for eight successive oxidation runs. Before each oxidation run a regeneration with nitrogen and hydrogen was applied *in situ* for 1.8×10^3 s at 323 K. The overnight N_2 treatments were applied by stirring the catalyst for 50×10^3 s in the reactor solution in a nitrogen atmosphere prior to the regeneration. Conditions: $C_{MGP} = 186$ mol m^{-3}, $C_{NaMG} = 6.5$ mol m^{-3}, pH $= 9$, $T = 323$ K, $p_{O_2} = 10^5$ Pa, $C_{cat} = 2$ kg m^{-3}.

DISCUSSION

The decrease of the CO chemisorption capacity upon aqueous phase reduction at high pH as shown in Fig. 5 is caused by two distinct phenomena. First, platinum particle growth is clearly observed with TEM and XRD as indicated in Table 1 by the H_2B-samples. Furthermore, the appearance of aggregates of platinum particles is shown in Fig. 6. Second, site covering is concluded from the fact that the calculated d_s^{CO} increased relatively more than d_s^{TEM} and d_w^{TEM}. Also, site covering is indicated by the increase of the fraction exposed if, subsequent to the reduction experiment, aqueous phase oxidation was applied as indicated in Table 1 by H_2B2-250R.

For the oxidation reaction of methyl α-D-glucopyranoside, site covering, platinum leaching, and particle growth have been shown to take place as a result of prolonged use of the catalyst (16, 18). In the present case the extent of deactivation by platinum leaching and particle growth is limited, whereas site covering causes a more extensive decrease of the reaction rate, indicated by the decrease of the FE^{CO} of sample M7 in Table 1.

Upon gas phase treatment at 773 K, platinum particle growth is limited in a hydrogen and nitrogen atmosphere, as indicated by H_2G and N_2G in Table 1. In an oxygen atmosphere, however, a large increase of the platinum particle diameter was observed as is clear from the O_2G data in Table 1.

Clearly, the mechanism according to which platinum particle growth and site covering occur strongly depends on the catalyst environment. The gas phase used during the gas and aqueous phase experiments and the pH in the aqueous phase experiments are two important variables determining the extent of particle growth and site covering.

Platinum Particle Growth

The decrease of the CO chemisorption capacity upon aqueous phase reduction is most predominant at high pH in a hydrogen atmosphere, as indicated in Fig. 4. The decrease of the FE^{CO} in Fig. 5 is partly caused by platinum particle growth as is clearly observed with TEM and XRD and indicated in Table 1 for the H_2B-samples by the increase of the average platinum particle diameter upon time of treatment. Also, from Fig. 2 it appears that the platinum particle diameter distributions are skewed toward the larger diameter side with increasing time of treatment. Furthermore, the appearance of aggregates of platinum particles was shown in Fig. 6.

In general, particle growth may occur by surface migration of platinum particles or atoms or by transport of platinum through the liquid phase. Transfer of platinum through the liquid phase is less likely, because under reducing conditions platinum ions that may dissolve are absent. Surface migration of platinum particles and platinum atoms are two distinct mechanisms, which are not mutually exclusive (27, 43–45). The first mechanism involves the random migration of particles resulting in collisions with other mobile or fixed particles, followed by their coalescence, which leads to particle growth. The other mechanism involves interparticle migration of atoms between fixed particles via the support surface. The first surface migration mechanism is termed particle migration and the second, which implies the migration of atoms, corresponds to Ostwald ripening (27).

The observation that the reductive treatment at pH = 13 is coupled with the appearance of aggregates of platinum particles favors the particle migration mechanism. In the aggregates shown in Fig. 6, individual particles can be observed, which are at the first stage of their coalescence. It was proposed by Wynblatt and Gjostein (43) that platinum particle migration may occur not by simultaneous translational motion of the whole crystallite, but by migration of platinum adatoms on the platinum surface resulting in an eventual transfer of platinum mass from one side of the particle to the other. This may lead to a change of the particle geometry and the formation of aggregates.

Besides the evidence for the particle surface migration mechanism obtained with TEM, other methods to distinguish between particle and adatom surface migration provide indications that the latter plays only a limited role.

First, for two-dimensional Ostwald ripening an initial increase of the exposed fraction of platinum atoms may be observed, because crystallites release atoms to the support surface (28). In the first part of Fig. 5, however, a rapid decrease of FE^{CO} is observed. Hence, this result gives no indication of Ostwald ripening, although a small initial increase of the fraction exposed may have been completely compensated by site coverage.

Second, the particle diameter distribution will be different for both particle growth mechanisms. For particle migration and subsequent coalescence a Gaussian distribution will become broader and skewed towards the larger particle diameter side. On the other hand, Ostwald ripening will result in a bimodal distribution (46). From Fig. 2 no bimodal distribution can be concluded, although the limited accuracy of the determination of the particle diameter distributions and the impossibility to detect particles below the detection limit of about 0.5 nm may cause problems in this respect (47).

Third, assuming that particle growth and aggregate formation are caused by particle surface migration, an attempt was made to estimate an average platinum particle migration distance, x, after a given time, t, and the corresponding particle diffusion coefficient, D_p. Comparison with literature data may then indicate whether the particle surface migration mechanism is realistic or not.

The above quantities are related by

$$D_p = \frac{x^2}{4\,t}. \qquad [6]$$

The average migration distance is estimated by calculating the distance from which particles must have migrated toward each other in order to create an aggregate. First, the number of particles which must have formed the aggregate was estimated. For the largest aggregate observed after 250×10^3 s of reduction at 363 K and pH = 13, which is shown in Fig. 6, it was estimated that 1.5×10^4 hemispherical particles with $d_n = 1.45$ nm must have formed the aggregate. Next, the number of those hemispherical platinum particles per unit of support surface area was calculated from the BET surface area of 1.02×10^5 m^2 kg_{cat}^{-1} and the platinum content of 3.4×10^{-2} kg_{Pt} kg_{cat}^{-1}. From the calculated value of 1 platinum particle per 50 nm^2 it follows that 1.5×10^4 platinum particles cover a surface area of 7.5×10^5 nm^2 on the fresh catalyst. If the aggregate is considered as the fixed center of a circle in which all platinum particles have formed the aggregate during the reduction experiment, the radius of that circle is 5×10^2 nm. If the average particle migration distance, x, is equal to the radius of this circle, calculation of the particle diffusion coefficient, D_p, from Eq. [6] gives

0.2×10^{-18} m^2 s^{-1}. This value is of the same order of magnitude but smaller than that found in gas phase sintering experiments at much higher temperatures. For example, for 2.5 nm platinum particles on alumina, which were annealed at 873 K for 5 h, a D_p of 1.5×10^{-18} m^2 s^{-1} was reported (43). Thus it can be concluded that on the basis of the calculated particle diffusion coefficient the particle surface migration mechanism is realistic.

Clearly, the aqueous phase plays an important role in the particle growth mechanism in a hydrogen atmosphere. Particle migration can occur at a much lower temperature in the liquid phase. Whereas in the gas phase in a hydrogen atmosphere at 773 K particle growth is limited as indicated in Table 1 by H$_2$G, the presence of an aqueous phase containing sodium hydroxide accelerates particle migration in a hydrogen atmosphere at 363 K. Moreover, a higher NaOH/catalyst ratio results in a larger average particle diameter as indicated by the data for sample H$_2$B1-250 in Table 1, which was treated at a higher NaOH/catalyst ratio than H$_2$B2-250. Chu and Ruckenstein (48) explained the increased sintering of platinum particles on a carbon film in gas phase at 773 K in the presence of water vapor to be a result of a decrease of the particle support interaction, speculating that the particles migrate by floating over the support. In the reduction experiments in aqueous phase the effect of water and hydroxide may be similar. The presence of the aqueous phase may accelerate the destruction of the oxygen-containing surface groups, destroying the platinum support interaction. Also, the support surface may be modified by reaction or interaction of hydroxide ions with the acidic support surface groups. Both effects will stimulate platinum particle surface migration and consequently particle growth. Another role of OH$^-$ might lie in its ability to permit transfer of platinum adatoms from the platinum surface to the graphite support (28, 43). In this way the transport of platinum particles on the support may be facilitated via a mechanism in which platinum particle migration occurs by movement of platinum adatoms on the platinum surface, resulting in a eventual transfer of platinum mass from one side of the particle to the other. This mechanism may also explain the formation of platinum aggregates.

During the oxidation of methyl α-D-glucopyranoside, particle growth is small and occurs only during the prereduction, which was performed in water at 363 K in a hydrogen atmosphere. The platinum particle diameter measured with TEM or XRD for M1, M4, and M7 in Table 1 shows a small increase compared to the fresh catalyst and no further increase is observed after the prereduction, indicated by sample H$_2$L. Also, small platinum aggregates are observed for the samples M1, M4, and M7 used for the oxidation reaction and the pre-reduced sample H$_2$L as shown in the TEM micrograph in Fig. 9 for sample M7. The near absence of particle growth under oxidizing conditions can be correlated with the results of Fig. 8, where after a nor-

mal regeneration procedure of 1.8×10^3 s the initial rate is completely restored. Hence, as particle growth takes place mainly under reducing conditions and platinum aggregates are observed, the mechanism for particle growth consists mainly of platinum particle migration, as was the case during the hydrogen treatment at pH $= 13$ and 363 K.

Platinum particle growth via a platinum particle migration mechanism also takes place upon gas phase oxidation at 773 K. A large increase of the platinum particle diameter is observed after treatment in an oxygen atmosphere at 773 K, whereas in a hydrogen or nitrogen atmosphere only a small increase is observed, as indicated in Table 1. Bett et al. (28) demonstrated that platinum supported on activated carbon required temperatures in excess of 873 K to bring about particle growth in a hydrogen and nitrogen atmosphere. Prado-Burguete et al. (49) showed that the oxygen-containing surface groups on the carbon support hamper the platinum particle growth in a hydrogen atmosphere at 773 K. In an oxygen atmosphere, however, platinum-catalyzed carbon burnoff (31) destroys the support together with the anchorage sites, causing platinum particle mobility and particle growth upon collision and coalescence of two particles.

From the gas and aqueous phase experiments it can be concluded that platinum particle growth can be attributed to the destruction of the strong interaction of the platinum particle with the graphite support. The oxygen-containing surface groups of the graphite support, which are responsible for this interaction, are able to inhibit platinum particle growth under mild conditions, e.g. those during the aqueous phase selective oxidation reaction. During hydrogen treatment in liquid phase, especially at high pH and high temperature, and during oxygen treatment in gas phase at 773 K, these surface groups are destroyed. This causes platinum particle mobility and via collision and coalescence there is particle growth.

It is interesting to compare the CO chemisorption data for small and large particles with the TEM data, without considering the data which are affected by site coverage. For the fresh catalyst the adsorption stoichiometry, calculated as d_s^{TEM}/d_s^{CO}, is 0.73. This value is in good agreement with literature data of Freel (42), who reported 0.85 for platinum on silica catalysts above a fraction exposed of 0.25, and Rodriguez-Reinoso et al. (41), who reported 0.62 for activated-carbon-supported platinum catalysts, also for FE > 0.25. For larger particles the difference between d_s^{TEM} and d_s^{CO} or d_w^{TEM} and d_w^{XRD} is smaller than for the fresh catalyst, as indicated in Table 1 for H$_2$G, N$_2$G, and O$_2$G. After the gas phase hydrogen treatment d_s^{TEM} is even larger than d_s^{CO}. Consequently, the CO adsorption stoichiometry reaches unity for larger particles. Rodriguez-Reinoso et al. (41) reported the same effect and proposed two explanations. First, electron transfer from the support toward platinum, which is more pronounced for smaller particles,

would facilitate bridge-bonded CO. Second, for small particles the fraction of platinum atoms at edges will be greater (50), favoring bridge-bonded CO. An increase of the fraction of bridge-bonded CO compared to the fraction of linear-bonded CO implies that for small particles the CO adsorption stoichiometry is smaller.

Site Covering

Site covering was observed to take place during the aqueous phase treatment at pH = 13 and 363 K. It is indicated by the increase of the CO chemisorption capacity of sample H$_2$B2-250 after four oxidation–reduction cycles. The fraction exposed recovered to 0.25 as indicated by sample H$_2$B2-250R in Table 1. It has been reported by Vleeming *et al.* (18) that the decrease of the fraction exposed upon hydrogen treatment at pH = 13 could also be partly recovered by potential cycling of the catalyst in an electrochemical setup and by heating in oxygen at 473 K. Another indication for site covering is that the d_s^{CO} increased from 2.3 nm to 14 nm, whereas the increase of the average platinum particle diameter measured with TEM and XRD is much smaller. In other words, the application of Eq. [5], converting the FE^{CO} to the d_s^{CO}, is actually not allowed in this case, because platinum surface atoms, which are covered, are not available for CO chemisorption.

The selective oxidation reaction of methyl α-D-glucopyranoside is only accompanied by site covering during the prereduction and the overnight stay of the catalyst in the reaction solution under nitrogen. As a result of the prereduction the fraction exposed decreases from 0.56 for the fresh catalyst to 0.41 for H$_2$L as given in Table 1. Applying the regeneration procedure for a relatively short time, a small or even no effect on the rate after regeneration is observed, but maintaining the catalyst overnight under reducing conditions clearly causes a decrease of the initial rate, as indicated in Fig. 8, and a decrease of the fraction exposed, as measured with CO chemisorption. The fraction exposed decreases from 0.41 for the catalyst prior to the first oxidation run to 0.27 for the catalyst after the last oxidation run (Table 1, M7). This decrease constitutes the main reason for the decrease of the initial rate in Fig. 8 with increasing number of overnight N$_2$ treatments.

Site covering during the overnight stay of the catalyst in the reaction solution can be caused by the presence of organic side products from the methyl α-D-glucopyranoside oxidation. Site covering as a result of the aqueous phase reduction at pH = 13 or the prereduction in water at 363 K must however be caused by products originating from the graphite support. It is assumed that as a result of the destruction of the oxygen-containing surface groups under reducing conditions, which caused platinum particle mobility and particle growth, products are formed which may cause covering of sites. The aqueous phase and the presence of sodium hydroxide in particular play an important role in this respect, because gas phase reduction only has a limited effect on the CO adsorption capacity. Furthermore, during aqueous phase reduction an increase of the NaOH/catalyst ratio results in a larger decrease of the FE^{CO}.

CONCLUSIONS

The extent of modifications of graphite-supported platinum catalysts due to particle growth and covering of metal sites strongly depends on the catalyst environment. Whereas in gas phase oxidation at 773 K platinum particle growth is largely due to sintering caused by extensive carbon burnoff of the graphite support, in the aqueous phase particle growth is limited during treatment in an oxygen atmosphere. In a nitrogen or hydrogen atmosphere at 773 K the increase of the particle diameter is small. However, aqueous phase reduction, especially at high pH and temperature, is responsible for the reduction of the oxygen-containing support surface groups, destroying the platinum anchorage sites. This enables platinum particle surface migration, which leads to the formation of platinum aggregates, particle growth, and site covering with products originating from the graphite support. The decrease of the initial rate for the oxidation of methyl α-D-glucopyranoside after reductive regeneration can be ascribed to covering of sites by side products or products originating from the graphite support under prolonged reducing conditions.

APPENDIX: NOTATION

Roman Symbols

b	Instrumental line broadening	radians
C	Concentration	mol m^{-3}
C_{cat}	Catalyst concentration	kg m^{-3}
D	Diffusion coefficient	m^2 s^{-1}
d	Diameter	m
FE	Fraction exposed	mol Pt$_s$(mol Pt)$^{-1}$
n	Number of particles	
n_i	Number of particles with diameter i	
p	Pressure	Pa
R_w^0	Initial specific consumption rate	mol kg$_{cat}^{-1}$ s^{-1}
T	Temperature	K
t	Time	s
x	Average migration distance	m

Greek Symbols

$\beta_{1/2}$	linewidth at half maximum	radians
θ	Bragg angle of incidence	degrees
λ	wavelength	nm
σ	standard deviation	

Subscripts

ads	Adsorbed
cat	Catalyst
i	of ith class
MGP	Methyl α-D-glucopyranoside
NaMG	Sodium 1-O-methyl α-D-glucuronate
n	Number averaged
O2	Oxygen
p	Particle
S	Surface
s	Surface area averaged
w	Weight averaged

Superscripts

CO	CO chemisorption
TEM	Transmission electron microscopy
XRD	X-ray diffraction
chem	Chemisorption technique

REFERENCES

1. Heyns, K., and Paulsen, H., *Adv. Carbohydr. Chem.* **17**, 169 (1962).
2. Röper, H., *in* "Carbohydrates as Raw Materials" (F. W. Lichtenthaler, Ed.), p. 267. VCH, Weinheim, 1991.
3. Van Bekkum, H., *in* "Carbohydrates as Raw Materials" (F. W. Lichtenthaler, Ed.), p. 289. VCH, Weinheim, 1991.
4. Mallat, T., and Baiker, A., *Catal. Today* **19**, 247 (1994).
5. Khan, M. I. A., Miwa, Y., Morita, S., and Okado, J., *Chem. Pharm. Bull.* **31**, 1141 (1983).
6. Khan, M. I. A., Miwa, Y., Morita, S., and Okado, J., *Chem. Pharm. Bull.* **31**, 1827 (1983).
7. Goodenough, J. B., Hamnett, A., Kennedy, B. J., and Weeks, S. A., *Electrochim. Acta* **32**, 1233 (1987).
8. Hronec, M., Cvengrosova, Z., Tuleja, J., and Ilavsky, J., *in* "New Developments in Selective Oxidation" (G. Centi and F. Trifirò, Eds.), Studies in Surface Science and Catalysis, Vol. 55, p. 169. Elsevier, Amsterdam, 1990.
9. Kimura, H., Kimura, A., Kokubo, I., Wakisaka, T., and Mitsuda, Y., *Appl. Catal. A: General* **95**, 143 (1993).
10. Mallat, T., Bodnar, Z., Brönnimann, C., and Baiker, A., *in* "Catalyst Deactivation 1994" (B. Delmon and G. F. Froment, Eds.), Studies in Surface Science and Catalysis, Vol. 88, p. 385. Elsevier, Amsterdam, 1994.
11. Nicoletti, J. W., and Whitesides, G. M., *J. Phys. Chem.* **93**, 759 (1989).
12. Mallat, T., Baiker, A., and Botz, L., *Appl. Catal. A: General* **86**, 147 (1992).
13. Dirkx, J. M. H., and van der Baan, H. S., *J. Catal.* **67**, 1 (1981).
14. Dirkx, J. M. H., and van der Baan, H. S., *J. Catal.* **67**, 14 (1981).
15. Dijkgraaf, P. J. M., Duisters, H. A. M., Kuster, B. F. M., and van der Wiele, K., *J. Catal.* **112**, 337 (1988).
16. Schuurman, Y., Kuster, B. F. M., van der Wiele, K., and Marin, G. B., *Appl. Catal. A: General* **89**, 47 (1992).
17. De Bruijn, F. A., Marin, G. B., Niemantsverdriet, J. W., Visscher, W. H. M., and van Veen, J. A. R., *Surf. Interface Anal.* **19**, 537 (1992).
18. Vleeming, J. H., De Bruijn, F. A., Kuster, B. F. M., and Marin, G. B., *in* "Catalyst Deactivation 1994" (B. Delmon and G. F. Froment, Eds.), Studies in Surface Science and Catalysis, Vol. 88, p. 467. Elsevier, Amsterdam, 1994.
19. Brönnimann, C., Bodnar, Z., Hug, P., Mallat, T., and Baiker, A., *J. Catal.* **150**, 199 (1994).
20. Van den Tillaart, J. A. A., Kuster, B. F. M., and Marin, G. B., *in* "Catalytic Selective Oxidation" (S. T. Oyama and J. W. Hightower, Eds.), ACS Symposium Series, Vol. 523, p. 299. ACS, Washington D. C., 1993.
21. Peukert, M., Coenen, F. P., and Bonzel, H. P., *Electrochim. Acta* **29**, 1305 (1984).
22. Abbadi, A., and van Bekkum, H., *J. Mol. Catal. A: Chemical* **97**, 111 (1995).
23. Smits, P. C. C., Kuster, B. F. M., van der Wiele, K., and van der Baan, H. S., *Appl. Catal.* **33**, 83 (1987).
24. Parsons, R., and VanderNoot, T., *J. Electroanal. Chem.* **257**, 9 (1988).
25. Bae, I. T., Xing, X., Liu, C. C., and Yeager, E., *J. Electroanal. Chem.* **284**, 335 (1990).
26. Pérez, J. M., Muñoz, E., Morallón, E., Cases, F., Vásquez, J. L., and Aldaz, A., *J. Electroanal. Chem.* **368**, 285 (1994).
27. Ross, P. N., *in* "Catalyst Deactivation" (E. E. Peterson and A. T. Bell, Eds.), Chemical Industries Series, Vol. 30, p. 165. Dekker, New York, 1987.
28. Bett, J. A. S., Kinoshita, K., and Stonehart, P., *J. Catal.* **41**, 124 (1976).
29. Connolly, J. F., Flannery, R. J., and Meyers, B. L., *J. Electrochem. Soc.* **114**, 241 (1967).
30. Richard, D., and Gallezot, P., *in* "Preparation of Catalysts IV" (B. Delmon, P. Grange, P. A. Jacobs, and G. Poncelet, Eds.), Studies in Surface Science and Catalysis, Vol. 31, p. 71. Elsevier, Amsterdam, 1987.
31. McKee, D. W., *in* "Chemistry and Physics of Carbon" (P. L. Walker and P. A. Thrower, Eds.), Vol. 16, p. 1. Dekker, New York, 1981.
32. Ayres, C. H., and Meyer, A. S., *Anal. Chem.* **23**, 299 (1951).
33. Charlot, C., "Les Méthodes de la Chimie Analytique." Masson, Paris, 1961.
34. Lemaître, J. L., Menon, P. G., and Delannay, F., *in* "Characterization of Heterogeneous Catalysts" (F. Delannay, Eds.), Chemical Industries Series, Vol. 15, p. 299. Dekker, New York, 1984.
35. Gallezot, P., *in* "Catalysis: Science and Technology" (J. R. Anderson and M. Boudart, Eds.), Vol. 5, p. 221. Springer, Berlin, 1984.
36. Sashital, S. R., Cohen, J. B., Burwell, R. L., and Butt, J. B., *J. Catal.* **50**, 479 (1977).
37. Bergeret, G., Gallezot, P., and Imelik, B., *J. Phys. Chem.* **85**, 411 (1981).
38. Scholten, J. J. F., Pijpers, A. P., and Hustings, A. M. L., *Catal. Rev.-Sci. Eng.* **27**, 151 (1985).
39. Scardi, P., and Antonucci, P. L., *J. Mater. Res.* **8**, 1829 (1993).
40. Klug, H. P., and Alexander, L. E., "X-Ray Diffraction Procedures for Polycrystalline and Amorphous Materials," p. 618. Wiley, New York, 1974.
41. Rodríguez-Reinoso, F., Rodríguez-Ramos, I., Moreno-Castilla, C., Guerrero-Ruiz, A., and López-González, J. D., *J. Catal.* **99**, 171 (1986).
42. Freel, J., *J. Catal.* **25**, 149 (1972).
43. Wynblatt, P., and Gjostein, N. A., *Prog. Solid State Chem.* **9**, 21 (1975).
44. Ehrburger, P., *Adv. Colloid Interface Sci.* **21**, 275 (1984).
45. Ruckenstein, E., and Sushumna, I., *in* "Hydrogen Effects in Catalysts" (Z. Paál and P. G. Menon, Eds.), Chemical Industries Series, Vol. 31, p. 259. Dekker, New York, 1988.
46. Baker, R. T. K., *in* "Catalyst Deactivation 1991" (C. H. Bartholomew and J. B. Butt, Eds.), p. 1. Elsevier, Amsterdam, 1991.
47. Flynn, P. C., Wanke, S. E., and Turner, P. S., *J. Catal.* **33**, 233 (1974).
48. Chu, Y. F., and Ruckenstein, E., *Surf. Sci.* **67**, 517 (1977).
49. Prado-Burguete, C., Linares-Solano, A., Rodríguez-Reinoso, F., and Salinas-Martínez de Lecea, C., *J. Catal.* **115**, 98 (1989).
50. Van Hardeveld, R., and Hartog, F., *Surf. Sci.* **15**, 189 (1969).